

Journal of Biomedical Optics

SPIEDigitalLibrary.org/jbo

***In planta* imaging of Δ^9 - tetrahydrocannabinolic acid in *Cannabis sativa L.* with hyperspectral coherent anti-Stokes Raman scattering microscopy**

Erik T. Garbacik
Roza P. Korai
Eric H. Frater
Jeroen P. Korterik
Cees Otto
Herman L. Offerhaus

In planta imaging of Δ^9 -tetrahydrocannabinolic acid in *Cannabis sativa L.* with hyperspectral coherent anti-Stokes Raman scattering microscopy

Erik T. Garbacia,^{a*} Roza P. Korai,^{a*} Eric H. Frater,^{a,c} Jeroen P. Korterik,^a Cees Otto,^b and Herman L. Offerhaus^a

^aUniversity of Twente, MESA+ Institute for Nanotechnology, Optical Sciences Group, 7500AE Enschede, The Netherlands

^bUniversity of Twente, MIRA Institute for Biomedical Technology and Technical Medicine, Medical Cell BioPhysics Group, 7500AE Enschede, The Netherlands

^cUniversity of Arizona, College of Optical Sciences, Tucson, Arizona 85721

Abstract. Nature has developed many pathways to produce medicinal products of extraordinary potency and specificity with significantly higher efficiencies than current synthetic methods can achieve. Identification of these mechanisms and their precise locations within plants could substantially increase the yield of a number of natural pharmaceuticals. We report label-free imaging of Δ^9 -tetrahydrocannabinolic acid (THCa) in *Cannabis sativa L.* using coherent anti-Stokes Raman scattering microscopy. In line with previous observations we find high concentrations of THCa in pistillate flowering bodies and relatively low amounts within flowering bracts. Surprisingly, we find differences in the local morphologies of the THCa-containing bodies: organelles within bracts are large, diffuse, and spheroidal, whereas in pistillate flowers they are generally compact, dense, and have heterogeneous structures. We have also identified two distinct vibrational signatures associated with THCa, both in pure crystalline form and within *Cannabis* plants; at present the exact natures of these spectra remain an open question. © The Authors. Published by SPIE under a Creative Commons Attribution 3.0 Unported License. Distribution or reproduction of this work in whole or in part requires full attribution of the original publication, including its DOI. [DOI: 10.1117/1.JBO.18.4.046009]

Keywords: coherent anti-Stokes Raman scattering; nonlinear optics; microscopy; hyperspectral; Cannabis sativa; tetrahydrocannabinolic acid.

Paper 12776RR received Dec. 5, 2012; revised manuscript received Mar. 10, 2013; accepted for publication Mar. 20, 2013; published online Apr. 15, 2013.

1 Introduction

Since ancient times it has been known that some plants confer medical benefits beyond simply providing essential nutrients. Modern drug discovery relies extensively on cues from naturally existing compounds,^{1,2} and research has been able to show that the mechanisms involved in the natural synthesis of these medicinal compounds are in many cases significantly more efficient and potent than industrial methods can achieve.³ In an effort to enhance the pharmacological effects of synthetic drugs, there has been a push to understand these biosynthetic pathways and the synergies between the various natural compounds.⁴

One problem facing researchers is the relative lack of techniques that can locate and identify compounds of interest *in vivo* with high spatial precision and without extensive sample modification. While they are powerful, typical analytic techniques such as gas chromatography, mass spectrometry, and high-performance liquid chromatography are uniformly destructive and provide minimal spatial resolution. Fluorescence microscopy, a widespread imaging technique for animal tissue, has yet to find significant applications in plant biology, partly due to endogenous chromophores that complicate data analysis. Popular label-free imaging methods that rely on molecular vibrations

for contrast have a number of drawbacks: infrared absorption is hampered by ubiquitous water absorption and poor spatial resolution, while spontaneous Raman scattering requires long acquisition times and can be saturated by native sample autofluorescence.

An alternate label-free imaging technique, coherent anti-Stokes Raman scattering (CARS), has been used for submicron confocal microscopy in a wide range of fields for over a decade.^{5–11} The primary advantages of CARS microscopy over other label-free techniques are its rapid imaging capabilities, which extend up to video rate,¹² and intrinsic confocality, allowing three-dimensional sectioning without descanning beams or the installation of pinholes. We recently introduced a technique for hyperspectral imaging that combines the imaging speed of CARS with the wide tunability of an optical parametric oscillator (OPO).¹³ This method enables us to acquire hyperspectral data spanning up to 350 cm^{-1} at a rate of up to one discrete frequency every 1.3 s for images with 512×512 spatial pixels. These spectra can be qualitatively classified according to their profiles, since fluorescence and the nonresonant CARS background have flat frequency responses over our scan range, while vibrational modes show up as sharp peaks.

The aim of this study was to use the capabilities of hyperspectral CARS microscopy to localize Δ^9 -tetrahydrocannabinolic acid (THCa) in *Cannabis sativa L.* The cannabinoids, of which THC is the most well known, are unique terpenophenols that only exist in *Cannabis* plants, and are widely recognized for a variety of medicinal properties, including analgesia and antiemeticism.¹⁴ The overall quantitative distributions of the cannabinoids and their precursors within *Cannabis* have

*These authors contributed equally to this work.

Address all correspondence to: Herman L. Offerhaus, University of Twente, MESA+ Institute for Nanotechnology, Optical Sciences Group, 7500AE Enschede, The Netherlands. Tel: 0031 53 489 1097; Fax: 0031 53 489 3511; E-mail: h.l.offerhaus@utwente.nl

been determined with multiple techniques¹⁵ and as functions of numerous growth and treatment conditions,¹⁶ with an emphasis on controlling the precise ratios of THC to other endogenous cannabinoids. However, these analytical techniques are uniformly destructive and cannot easily provide chemical specificity at the micron level. One study fluorescently labeled the enzymes involved in THCa production, but did not directly image the cannabinoid.¹⁷ Because certain sections of the *Cannabis* plant are reported to contain up to 25%/w THCa,¹⁸ we have used it as a first demonstration of hyperspectral CARS on botanical samples. We have found that, in agreement with published reports,^{19,20} THCa is most densely localized within glandular trichomes on the flowering bodies of female plants. Furthermore, we have observed that the morphologies of THCa-containing organelles within individual trichomes are highly variable.

2 Materials and Methods

2.1 *Cannabis sativa* L. and Δ^9 -Tetrahydrocannabinolic Acid

Samples of dried female *Cannabis sativa* L. plants, consisting primarily of pistillate flowers and adjacent bracts, were obtained from a local distributor in Enschede, The Netherlands. White-light reflection stereomicroscopy was used to verify the presence and density of glandular trichomes and to identify structures of interest. Small sections of the pistils were removed from the central flower, with great care taken to ensure that the regions to be imaged were not damaged. Small leaves were likewise separated from the flower at the bases of their stems. These samples were immersed in deionized water to mitigate thermal effects and sealed between two clean #1 cover glasses. Slight morphological changes of the samples due to rehydration were observed, but did not affect the CARS measurements. The distributions and concentrations of cannabinoids within the samples were not expected to be modified because of the hydrophobicity of the cannabinoids.

For reference spectra we used >97% purity (as measured with HPLC and ¹H-NMR) crystalline THCa (39382-10MG; Sigma Aldrich), which was stored at -20°C. Immediately before imaging we sealed a small amount of THCa in air between two clean #1 cover glasses. Care was taken to avoid contamination. New samples were prepared for each imaging session.

2.2 Optical Setup

Our optical setup has been described in depth elsewhere.¹³ Briefly, a frequency-doubled Nd:YVO₄ laser (Paladin; Coherent, Inc.) synchronously pumped an OPO (Levante Emerald; APE Berlin GmbH), producing two dependently tunable near-IR beams. For imaging the *Cannabis* plants we used the signal beam from the OPO, nominally centered around 810 nm, combined with the laser fundamental at 1064 nm to excite high-frequency alkyl vibrations near 3000 cm⁻¹. To obtain spectra of the pure THCa crystals we used the OPO signal and OPO idler beams together, nominally centered at 920 and 1260 nm, respectively. The latter pair provided up to 350 cm⁻¹ of tuning bandwidth, twice that of the signal-1064 combination. The selected pair of beams was sent collinearly into an inverted laser-scanning microscope (IX71/FV300; Olympus) and focused into the sample with a 60 × 1.2 NA water immersion objective (UPLSAPO 60XW/IR; Olympus). Transmitted CARS signals were collected with a long-working-distance 0.55 NA

objective (MWUCD; Olympus), spectrally filtered to reject the pump and Stokes beams (Chroma HQ660/40 for the plants, Semrock FF01-716/43 for the pure THCa), and detected on a photomultiplier tube (R3986; Hamamatsu). Back-scattered CARS signals were reflected off of a dichroic mirror (FF775; Semrock), and filtered and detected with identical but separate components as the transmitted CARS signal.

Two-photon-excited autofluorescence from the wide variety of native fluorophores in the plants can be a problem in CARS experiments. Chlorophyll a, for example, has a very strong absorption band in the blue, but only weakly absorbs in the green. For plant imaging we used the OPO signal (~820 nm) as the pump beam in the CARS process and the laser fundamental (1064 nm) as the Stokes beam. The second harmonic of the pump beam, around 410 nm, is strongly absorbed by chlorophyll a, while the sum-frequency of the pump and Stokes beams at 470 nm and the second harmonic of the Stokes beam at 532 nm are not. To separate these processes we switched the laser fundamental beam on and off at high frequency (2.4 MHz) with an acousto-optic modulator. The light emitted from the sample then contained two components: a fluorescent DC component from two-photon absorption of the pump beam and an AC component at 2.4 MHz with the CARS signal and fluorescence from the other two-photon absorptions, both of which were recorded on the PMT. The output of the detector was sent to a high-speed lock-in amplifier (HF2LI; Zurich Instruments), where the large DC component was filtered out, leaving only the CARS signal and residual fluorescence. We used a high modulation frequency and short time constant (5 μs) on the lock-in amplifier to maintain a fairly high imaging rate.

For hyperspectral CARS imaging we scanned the laser beams over the sample to create a two-dimensional image (frame) at one vibrational frequency, then slightly changed the orientation of a Lyot filter inside the OPO cavity between frames to shift to the next frequency. The minimum frequency shift is 0.7 cm⁻¹, though for speed considerations we used 2 cm⁻¹ intervals. Many iterations of this process generated the full hyperspectral datacube. An image processing algorithm projected this three-dimensional datacube into a color-coded two-dimensional image wherein each spectrum is uniquely and qualitatively represented. Specific regions of interest were then selected based on visual inspection of these projections, from which CARS spectra were extracted from the original datacube. These spectra were corrected in post-processing for variations in pump and Stokes beam power.

3 Results and Discussion

3.1 Δ^9 -Tetrahydrocannabinolic Acid

To determine the spectral markers for locating THCa in our experiments in *Cannabis sativa* L. plants, we first obtained reference spectra of pure crystalline THCa. A representative hyperspectral image projection is shown in Fig. 1(a), with the spectra of the indicated regions shown in Fig. 1(b). This image of 256 × 256 pixels at 117 spectral points was recorded in 2 min. Surprisingly, we find two unique spectra associated with pure THCa, which we call THC₁ and THC₂. The THC₁ spectrum (blue region and curve) contains many overlapping alkyl vibrational modes, with four major peaks located at 2825, 2868, 2907, and 2940 cm⁻¹, while the THC₂ spectrum (red region and curve) has a single prominent feature at 2903 cm⁻¹ and a minor secondary peak at 2960 cm⁻¹. Based

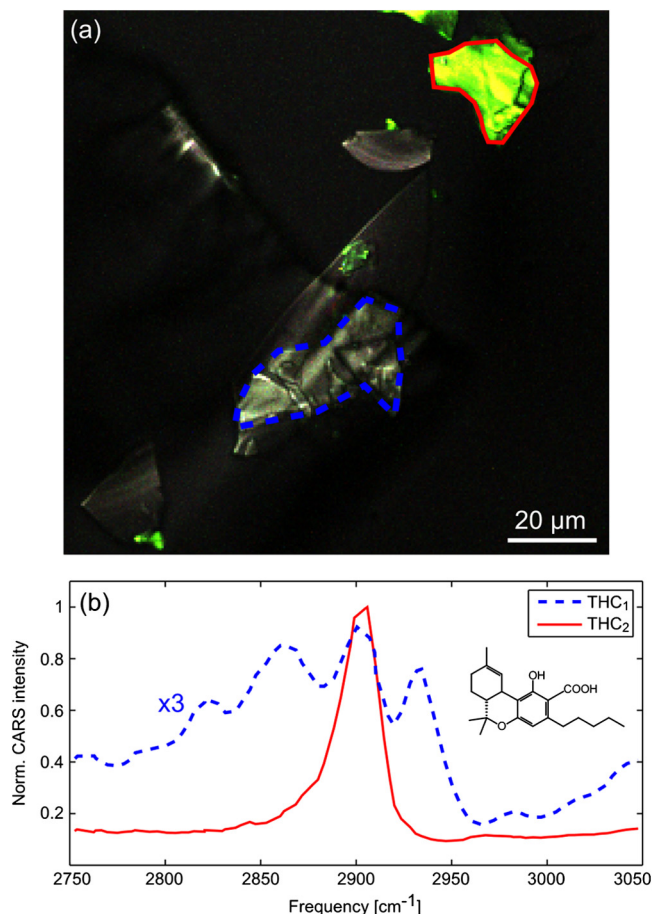


Fig. 1 (a) Hyperspectral CARS image of pure THCa crystals displaying two distinct colors. (b) Spectra extracted from the indicated regions of (a). Key marker frequencies for THC_1 are 2825, 2860, 2905, and 2940 cm^{-1} , while THC_2 has only a single strong peak at 2900 cm^{-1} . Small inclusions of THC_2 within the blue region generate additional intensity at 2900 cm^{-1} in the THC_1 spectrum. The THCa structure is shown in part (b). Note that both spectra in part (b) have been normalized to the maximum value of the THC_2 spectrum, and that the THC_1 spectrum has been scaled by an additional factor of three.

on the structure of the THCa molecule we expect a complicated vibrational spectrum with significant contributions from both CH_2 and CH_3 modes, which we can reconcile with THC_1 (blue curve), although specific band assignments are not attempted. The THC_2 spectrum (red curve) is especially interesting because this spectrum was represented in approximately half of the THCa crystals that we measured. Both spectra are insensitive to the orientations of the crystals relative to the polarizations of the laser beams, indicating that these two spectra do not arise from a systematic measurement artifact, and the crystals of THC_1 and THC_2 are indistinguishable under white-light illumination. From these observations and the HPLC and $^1\text{H-NMR}$ data, we propose that these two spectra correspond to two distinct crystal solid-state forms of THCa. Large variations in the vibrational spectra between multiple crystal forms of the same compound are not unheard-of, as has been shown with spontaneous Raman for mannitol²¹ and lactose.²²

3.2 *Cannabis sativa* (Leaf)

To measure THCa within the leaves of a *Cannabis* plant we detect the back-scattered CARS signal, since strong absorption

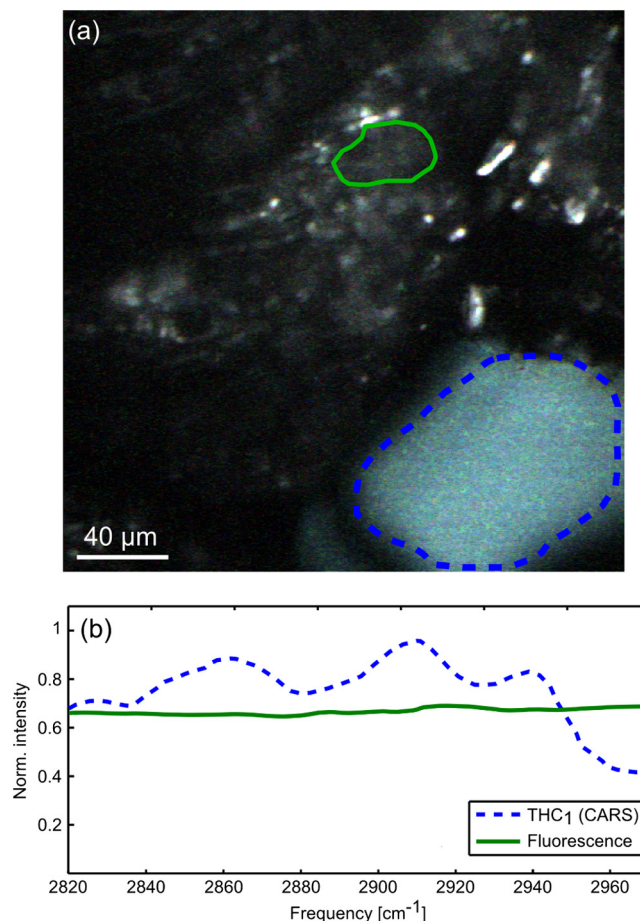


Fig. 2 Hyperspectral CARS image (a) and spectra (b) from a *Cannabis sativa* L. leaf, recorded in reflection, showing native fluorescence (green region and curve) and a THC_1 CARS signal (blue region and curve).

of the 650-nm anti-Stokes emission by chlorophyll and high losses due to scattering in the leaves precluded detection in transmission. The presence of numerous fluorescent bodies necessitated use of modulated detection. A representative hyper-spectral image, consisting of 512×512 pixels over 80 spectral points and imaged at 7 s per frame, is shown in Fig. 2(a), with spectra of the indicated regions in Fig. 2(b).

Immediately obvious from Fig. 2 is that the two highlighted regions have very dissimilar spectral profiles. The region indicated in blue is spectrally very close to that of pure THC_1 , while the region outlined in green shows the flat, featureless spectral curve typical of fluorescence. We believe that this fluorescence is mostly from chlorophyll b, which can be excited by the simultaneous absorption of one pump photon and one (modulated) Stokes photon and whose emission is therefore modulated.

The physical morphology also differs between the THC_1 and fluorescent regions, with the former appearing spatially more homogeneous and having smoother edges than the latter. The spatial features of the THC_1 signal appear generally consistent with a storage vesicle or reservoir. Small irregularities of the edges of this region may indicate a rupture of the vesicle that has allowed the THC_1 to diffuse into the surrounding tissue and deformed the walls of the vesicle. The lack of other spectral signatures in the THC_1 region points toward a relatively high purity and local concentration of cannabinoids, and the absence of a discernible microscopic structure indicates either a solvated or nano-crystalline phase.

3.3 *Cannabis sativa* (Pistil)

The pistils of flowering *Cannabis* plants are known to contain large quantities of cannabinoids, with average concentrations of 10 to 12%/w (see Ref. 17). We have observed that, unlike the leaves, pistils contain very dense distributions of cannabinoids in complicated heterogeneous structures. Because the pistils are fairly thin and their glandular trichomes are nearly transparent, CARS detection in transmission is utilized. This confers two advantages: CARS emissions are highly directional, with a strong preference for scattering forward in a relatively narrow cone, and so are efficiently collected and relayed to detectors in that direction; and CARS emissions coherently add as the beams propagate through a sample, by which process the signals from large objects (those larger than the wavelength of light) benefit tremendously.

Most of the THCa signals that we have recorded appear to originate in structures with linear dimensions greater than $1\ \mu\text{m}$, as illustrated by the z-stack series in Fig. 3. To create this image the laser focus was axially translated by $1\ \mu\text{m}$ through the sample between individual frames. A total of 60 frames were recorded at a constant vibrational frequency of $2940\ \text{cm}^{-1}$. Each frame was recorded in 10 s, including three averages. We verified that the bright signals correspond to a THC_1 CARS signals by taking a hyperspectral image (not shown) at a slice in the center of the stack. To depict the three-dimensional structure of the entire trichome we have applied a z-dependent color to each slice (from the Z-Stack functions of the MBF library in ImageJ). The hazy background in the top half of the image is the nonresonant background of the water immersion medium. Reds and yellows indicate regions toward the bottom of the stack, while blues and purples are at the top of the stack. There are four distinct regions that can be identified. The red/orange section at top right is highly structured and dense, and contains small voids or vacuoles. Directly beneath that section are two unconnected regions of similar morphology at different

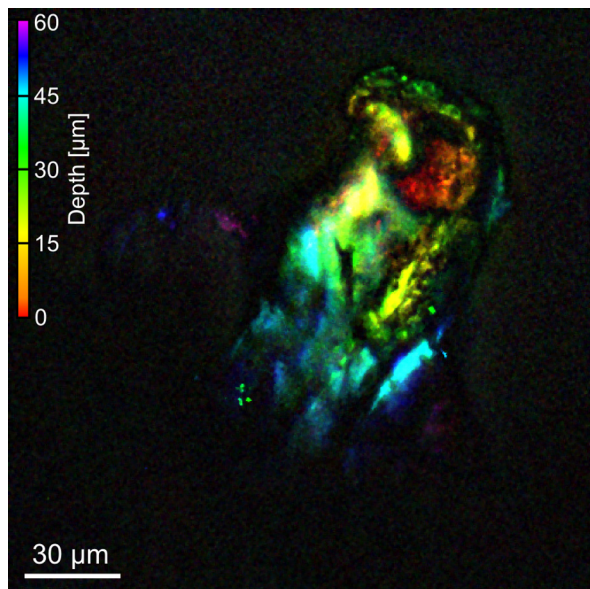


Fig. 3 Color-coded projection of a CARS z-stack in a glandular trichome, measured at the THC_1 peak at $2940\ \text{cm}^{-1}$. Reds and oranges indicate the bottom of the stack, while blues and purples are at the top of the stack. Many different physical morphologies are visible at different regions within this trichome.

heights in the sample, colored yellow/green and light blue, respectively. These regions contain higher concentrations of cannabinoids, but in elongated and narrow structures. The left side of the trichome displays a large and more diffuse distribution without clear and sharp boundaries (yellow, green, light blue), similar to that observed in the bract. Finally, the far top right of the trichome has a number of very thin regions of cannabinoids, shown in green, that may be closely associated with or bound to cell membranes. From these images the compartmentalized distribution of the cannabinoids is readily apparent. The observation of these different morphologies has not, to the best of our knowledge, been previously reported.

We have also imaged a region within an intact stigma of a female flower that contains both THC_1 and THC_2 in close proximity. The hyperspectral CARS image shown in Fig. 4 was recorded at a depth of about $30\ \mu\text{m}$, with $512 \times 512 \times 80$ pixels at 10 s per frame. The spectra from the magenta and blue regions of the image correspond approximately to THC_1 and THC_2 , respectively, and are shown in Fig. 4(b). Additionally, a small volume of a native lipid, which is easily identified by its characteristic CH_2 symmetric stretch at $2845\ \text{cm}^{-1}$, is outlined in green. Deviations from the reference spectrum of THC_1 can be attributed to the presence of other molecules in

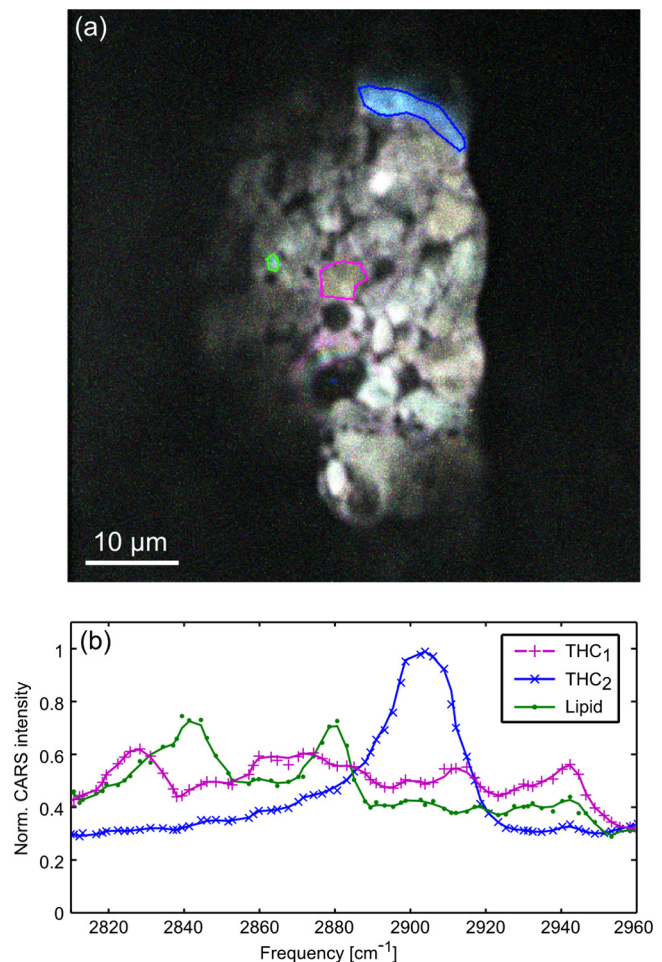


Fig. 4 Hyperspectral CARS image (a) and CARS spectra (b) of the interior of a stigma showing both representative THCa spectra (magenta and blue regions and curves) as well as native lipids (green region and curve). The presence of many compounds other than THCa in this section of the plant yields a complex mixture, from which it is impossible to find a pure THCa spectrum in any region of interest.

the focal volume of the laser beam, including other cannabinoids such as cannabidiol and cannabidiol.¹⁴ The broadening of the THC₂ peak is a result of detector saturation, a side effect of increasing the contrast of other regions in the image. At nonsaturated gain settings the spectrum is nearly identical to that shown in Fig. 1(b) for THC₂.

4 Conclusions

We have performed label-free, *in planta* measurements of THCa in *Cannabis sativa* L. with hyperspectral CARS microscopy. Our results confirm that cannabinoids are present in high concentrations in the glandular trichomes of female flowers, and show that the local distribution of THCa is morphologically diverse as a function of location within the plant: THCa-containing organelles within leaves tend to be large, spheroidal, and lack clear boundaries, while those within pistillate glandular trichomes are dense, irregularly shaped, and have distinct three-dimensional structures. In light of these results we expect that hyperspectral CARS microscopy will be a powerful tool in research of natural medicinal compounds.

Acknowledgments

Funding for this research was provided by the Nederlandse Wetenschappelijke Organisatie. The authors acknowledge K. J. Gorter, S. R. Visser, and M. K. Vreman for assistance with sample preparation; S. Kroes for many useful discussions; and A. L. Fussell for critical reading of our manuscript. The authors thank Coherent, Inc. for use of the Paladin laser and APE Berlin GmbH for the Levante Emerald OPO.

References

1. D. J. Newman, G. M. Cragg, and K. M. Snader, "Natural products as sources of new drugs over the period 1981–2002," *J. Nat. Prod.* **66**(7), 1022–1037 (2003).
2. M. S. Butler, "The role of natural product chemistry in drug discovery," *J. Nat. Prod.* **67**(12), 2141–2153 (2004).
3. I. Paterson and E. A. Anderson, "The renaissance of natural products as drug candidates," *Science* **310**(5747), 451–453 (2005).
4. J. M. McPartland and E. B. Russo, "Cannabis and cannabis extracts: greater than the sum of their parts?," *J. Cannabis Therapeut.* **1**(3/4), 103–132 (2001).
5. M. Windbergs et al., "Chemical imaging of oral solid dosage forms and changes upon dissolution using coherent anti-Stokes Raman scattering microscopy," *Anal. Chem.* **81**(6), 2085–2091 (2009).
6. E. Bélanger et al., "Quantitative myelin imaging with coherent anti-Stokes Raman scattering microscopy: alleviating the excitation polarization dependence with circularly polarized laser beams," *Opt. Express* **17**(21), 18419–18432 (2009).
7. C. Brackmann et al., "Visualization of β -carotene and starch granules in plant cells using CARS and SHG microscopy," *J. Raman Spectrosc.* **42**(4), 586–592 (2011).
8. G. W. H. Wurpel, H. A. Rinia, and M. Müller, "Imaging orientational order and lipid density in multilamellar vesicles with multiplex CARS microscope," *J. Microsc.* **218**(1), 37–45 (2005).
9. A. Conovaloff et al., "Imaging growth of neuritis in conditioned hydrogel by coherent anti-Stokes Raman scattering microscopy," *Organogenesis* **5**(4), 149–155 (2009).
10. R. S. Lim et al., "Identification of cholesterol crystals in plaques of atherosclerotic mice using hyperspectral CARS imaging," *J. Lipid Res.* **52**, 2177–2186 (2011).
11. N. L. Garrett et al., "Exploring uptake mechanisms of oral nanomedicines using multimodal nonlinear optical microscopy," *J. Biophotonics* **5**(5–6), 458–468 (2012).
12. C. L. Evans et al., "Chemical imaging of tissue *in vivo* with video-rate coherent anti-Stokes Raman scattering microscopy," *Proc. Natl. Acad. Sci. U.S.A.* **102**(46), 16807–16812 (2005).
13. E. T. Garbacik et al., "Rapid identification of heterogeneous mixture components with hyperspectral coherent anti-Stokes Raman scattering imaging," *J. Raman Spectrosc.* **43**(5), 651–655 (2012).
14. D. Baker et al., "The therapeutic potential of cannabis," *Lancet Neurol.* **2**(5), 291–298 (2003).
15. M. A. ElSohly and D. Slade, "Chemical constituents of marijuana: the complex mixture of natural cannabinoids," *Life Sci.* **78**(5), 539–548 (2005).
16. B. G. De Backer et al., "Innovative development and validation of an HPLC/DAD method for the qualitative and quantitative determination of major cannabinoids in cannabis plant material," *J. Chromatogr. B* **877**(32), 4115–4124 (2009).
17. S. Sirikantaramas et al., "Tetrahydrocannabinolic acid synthase, the enzyme controlling marijuana psychoactivity, is secreted into the storage cavity of the glandular trichomes," *Plant Cell Physiol.* **46**(9), 1578–1582 (2005).
18. B. G. De Backer et al., "Evolution of the content of THC and other major cannabinoids in drug-type cannabis cuttings and seedlings during growth of plants," *J. Forens. Sci.* **57**(4), 918–922 (2012).
19. J. E. Pitts, J. D. Neal, and T. A. Gough, "Some features of Cannabis plants grown in the United Kingdom from seeds of known origin," *J. Pharm. Pharmacol.* **44**(12), 947–951 (1992).
20. V. S. Lanyon, J. C. Turner, and P. G. Mahlburg, "Quantitative analysis of cannabinoids in the secretory product from capitulate-stalked glands of Cannabis sativa L. Cannabaceae," *Bot. Gazette* **142**, 316–319 (1981).
21. J. R. Beattie et al., "Investigation into the subambient behavior of aqueous mannitol solutions using temperature-controlled Raman microscopy," *Eur. J. Pharm. Biopharm.* **67**(2), 569–578 (2007).
22. J. H. Kirk, S. E. Dann, and C. G. Blatchford, "Lactose: a definitive guide to polymorph determination," *Int. J. Pharmaceut.* **334**(1–2), 103–114 (2007).